

The M_w 6.4 Damas, Costa Rica, Earthquake of 20 November 2004: Aftershocks and Slip Distribution

by Javier Fco. Pacheco, Ronnie Quintero, Floribeth Vega, Juan Segura,
Walter Jiménez, and Víctor González

Abstract The earthquake of 20 November 2004 was located north of Damas Island in the Pacific coast of Costa Rica, within the Costa Rica Deformed Belt. The earthquake was located at 24 km depth and reported with a magnitude (M_w) of 6.4 and a strike-slip mechanism with a large normal dip-slip motion. This mechanism agrees with mapped faults in the area that suggest transtensional deformation on the forearc and the entire western boundary of the Panama microplate. Aftershock locations do not delineate a preferable plane to distinguish between the two nodal planes and are distributed between 15 and 25 km depth. The slip distribution during the mainshock, modeled after teleseismic and local data, pictured a circular rupture 8 km in radius and 0.25 m of average displacement. The fault plane cannot be distinguished from the two nodal planes from the slip distribution because of the lack of directivity and resolution for this magnitude earthquake. Weak evidence from empirical Green's function analysis suggests that the dextral northwest-oriented fault could be the causative fault. Depth to the top of the slab, hypocenter location of the mainshock, its slip distribution, depth distribution of the aftershocks, and Quaternary fault activity at the surface suggest that deformation takes place throughout the whole thickness of the crust. This extended deformation might be caused by seamount subduction and strong basal friction on the upper plate, due to subduction of a thick, young, and buoyant oceanic plate, rough seafloor, and underplating of large seamounts.

Introduction

On 20, November 2004, a moderate earthquake caused extensive damage to the Central-Pacific coastal areas of Costa Rica, between the towns of Parrita and Quepos (Fig. 1). The earthquake occurred at 02:07 a.m. local time (08:07 UTC). Damage in Parrita and Damas Island was associated with extensive liquefaction and ground failure, while it was strongly felt throughout the rest of the country. The highest intensity (Mercalli Modified) reached VII at the epicentral area and V in the Central Valley, 50 km to the north of the epicenter. The closest accelerograph, QSP, located in the city of Quepos, 10 km from the epicenter, recorded a peak acceleration of 226 gal (Laboratorio de Ingeniería Sísmica, www.fing.ucr.ac.cr, 2005). The local seismic network (Güendel *et al.*, 1989) operated by the Costa Rica Volcanological and Seismological Observatory, at the National University (OVSICORI-UNA), reported the hypocenter at 25 km depth and 5 km inland from the coast. Harvard's Centroid Moment Tensor (CMT) Solution (Dziewonski and Woodhouse, 1983; Harvard Seismology, 2005) reported a moment magnitude M_w 6.4 and a centroid depth of 22 km. The causative fault, from Harvard's best double-

couple solution (Fig. 1), is either a steeply dipping, right-lateral strike-slip fault striking to the northwest (strike 305° , dip 78° , rake -138°) or a left-lateral fault striking to the northeast (strike 204° , dip 49° , rake -16°).

Although both hypocenter and centroid depth seem deep for a crustal event, they are too shallow to be associated with seismic activity at the plate interface or within the subducted Cocos plate. At the coast, in Central Costa Rica, Protti *et al.* (1995a) determined the plate interface to be between 30 and 40 km depth. More recent studies place the plate interface about 25 km below the coast. Stavenhagen *et al.* (1998) combined on- and offshore wide-angle seismic data along a profile just 40 km to the southeast of Quepos. Their high-resolution seismic profile placed the plate interface at 25 km just below the coast. DeShon *et al.* (2003) located the aftershocks of the shallow thrust event of 20 August 1999, Quepos earthquake (M_w 6.9) that occurred just to the southeast of the 2004 Damas earthquake. Using arrival-time data from a temporary array of inland and ocean-bottom seismometers, they were able to determine a 3D velocity model and delineate the geometry of the seismogenic zone

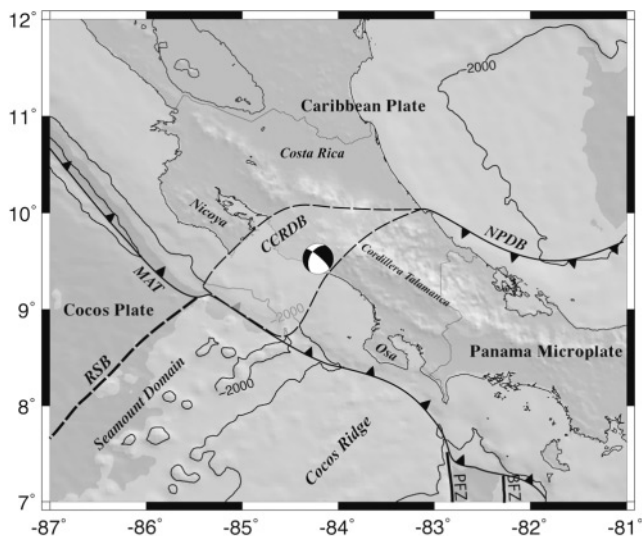


Figure 1. Tectonic map of Costa Rica. Middle American Trench (MAT), Central Costa Rica Deformed Belt (CCRDB), North Panama Deformed Belt (NPDB), Rough-smooth boundary (RSB), Panama Fracture Zone (PFZ), Balboa Fracture Zone (BFZ). Nicoya and Osa Peninsulas are also indicated. Focal mechanism from Harvard CMT solution shows the location of the mainshock.

with the relocated seismicity. With this high-resolution image, they find that the plate interface below the coast lies between 25 and 30 km depth. A tomography study, with selected P -wave arrival times from local and regional networks, by Husen *et al.* (2003), determined similar depths for the plate interface at cross sections close to the Damas and Quepos earthquakes. Hence, the hypocenter of the Damas earthquake probably lies in the lower crust, very close to and above the slab.

Ubiquitous surface breaks in the epicentral area were associated with ground failure due to soil conditions, and none had fault surface rupture (M. Mora, personal comm., 2005). The lack of surface rupture is consistent with rupture at greater depth. Nevertheless, active Quaternary faults with fault planes similar to the nodal planes obtained by Harvard for the Damas event have been mapped at the surface throughout the area (Marshall *et al.*, 2000; Denyer *et al.*, 2003). The large (M_s 7.0) San Casimiro earthquake of 4 March 1924, caused ground failure and liquefaction similar to that caused by the Damas event. However, in this case surface breaks were observed along a similarly oriented, to the northeast, but much larger fault (Montero, 1999).

We studied the seismicity following the mainshock and its slip distribution to determine the depth of rupture and causative fault plane.

Tectonic Setting

The interactions of two major plates, Cocos and Caribbean, and the Panama microplate are responsible for the high

rates of seismicity in Central Pacific Costa Rica (Fig. 1). The Cocos plate is currently being subducted underneath the Caribbean and the Panama microplate at a rate between 85 and 90 mm/yr (DeMets *et al.*, 1990) in a direction almost perpendicular to the Middle America Trench (MAT). Protti *et al.* (1994) classifies this part of the Middle American subduction zone as seismically decoupled because of high rates of seismicity and the absence of very large subduction zone earthquakes.

A broad zone of deformation, the Central Costa Rica Deformed Belt (CCRDB), defines the western Panama microplate boundary (Fisher *et al.*, 1994; Marshall *et al.*, 2000). Deformation along this broad boundary in central Costa Rica occurs along a diffuse array of conjugate faults of northwest-striking dextral and northeast-striking sinistral faults (Arias and Denyer, 1991; Fernández, 1996; Fernández and Pacheco, 1998; Marshall *et al.*, 2000). Most northeast-striking sinistral faults have lengths of up to 20 km, whereas northwest-striking dextral faults could reach up to 40 km in length (Marshall *et al.*, 2000). Close to the coast, within the inner forearc, deformation is carried out by a series of steep margin-perpendicular faults, along river valleys striking northeast, which allow for differential uplift of a system of inner forearc blocks (Fisher *et al.*, 1994, 1998; Marshall *et al.*, 2000). One of these faults, the northeast-oriented Tarcoles fault, ruptured during the 1924 San Casimiro earthquake (Montero, 1999). Some authors attribute this block system to the current subduction and underplating of seamounts (Fisher *et al.*, 1998; Marshall *et al.*, 2000).

The western boundary of the CCRDB coincides with the oceanic rough-smooth boundary (RSB) that separates smooth ocean floor created at the East Pacific Rise (EPR), a fast-spreading ridge, and the seamount domain (Hey, 1977; von Huene *et al.*, 1995, 2000) or rough seafloor originating at the Cocos-Nazca Spreading Center (CNSC), a slow-spreading ridge. Although studies by Barckhausen *et al.* (2001) place the RSB between the CNS-1, seafloor created at the CNSC, and CNS-2, seafloor created at the CNSC and overprinted by the Galapagos hot-spot-related volcanism. Seafloor to the southeast of the RSB is younger and more buoyant than seafloor to the northwest (Protti *et al.*, 1995a). Oceanic crust southeast of the RSB was overprinted by the Galapagos hot spot, which thickened the crust (Stavenhagen *et al.*, 1998) and produced many seamounts with the Galapagos hot-spot geochemistry (Werner *et al.*, 1999). Typical seamounts reach highs of 1.5 to 2.5 km. Seamounts disrupt the continental slope and can be traced below a 5-km-thick upper crust with swath map data (von Huene *et al.*, 2000). In a tomographic study, Husen *et al.* (2002) found evidence for an unperturbed subducted seamount beneath the continent at 30 km depth. This seamount coincides with the rupture area of the 25 March 1990 Cobano earthquake (M_w 7.0), a thrust earthquake along the plate interface (Protti *et al.*, 1995b). Both, Protti *et al.* (1995b) and Husen *et al.* (2002) interpreted the subducted seamount as an asperity whose rupture caused the Cobano event.

Mainshock and Aftershock Location

The Observatorio Volcanológico y Sismológico de Costa Rica (OVSICORI-UNA) has run a short-period seismic network since 1984 and has recently upgraded the network with five broadband stations (Guralp CMG-6TD) distributed in central Costa Rica (Fig. 2). Both short-period and broadband seismographs saturated during the Damas mainshock of 20 November 2004, but most aftershocks produced unsaturated records with good quality P and S readings.

The mainshock was located 12 km northwest of Parrita and 10 km northeast from the city of Quepos (Fig. 3). The depth of the mainshock was constrained with $S-P$ time readings from strong-motion stations operated by the Laboratorio de Ingeniería Sísmica (LIS-INII) of the University of Costa Rica. The strong-motion station located in the city of Quepos, QSP (Fig. 3), is located less than 12 km from the epicenter, giving a good control on the depth of this earthquake.

Routine locations are produced with the Seisan System of Lienert and Haskov (1995), and a 1D velocity model obtained by Quintero and Kissling (2001). In Figure 2 we present the first two weeks of activity recorded by the seismic network (a total of 550 events). Aftershocks are located between 5 and 30 km depth and there is no apparent alignment of the seismicity with either of the nodal planes from Harvard's CMT double-couple solution (striking 204° or 305°). To determine depth errors in location we generate synthetic readings, with a 3D crustal model (Husen *et al.*, 2002), for earthquakes located in the region, and then relocate them with the Seisan System and the 1D model of Quintero and Kissling (2001). Depth errors measured this way are less than 5 km.

We improved locations using the double-difference algorithm of Waldhauser and Ellsworth (2000). Given the proximity of the events and the large distances between events and stations we expect to improve locations using the differences in travel times between events and stations, correcting for large crustal velocity heterogeneities in the path. We obtain travel-time differences for each event pair with a separation distance less than 8 km at stations that are located within 200 km distance from the cluster centroid (which includes all the seismic network). A total of 364 events were selected, after pair match and distance distribution, for relocation. These relocated earthquakes are distributed between 15 and 25 km depth (Fig. 3). Although there is an improvement in the locations, measured by lower time residuals and a more compact distribution of the hypocenters, there is still no clear alignment of the aftershocks with either of the two nodal planes (Fig. 3). To test whether station distribution might strongly affect the location of the events we relocated the events without readings from the closest short-period station, QPSR, but found neither a large decrease nor an increase in location quality.

To determine whether the station distribution might be a limitation in the location of earthquakes in the area, we

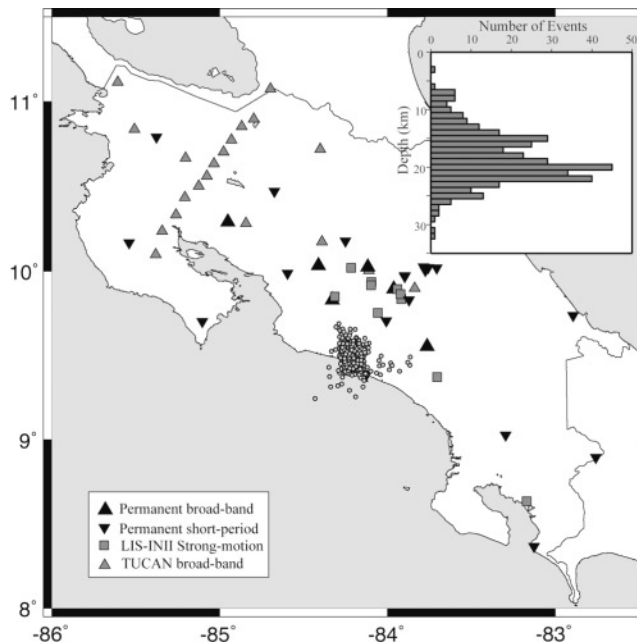


Figure 2. Earthquake locations and seismic stations used in this study. Inset with the depth distribution of the seismicity and different seismic network symbols.

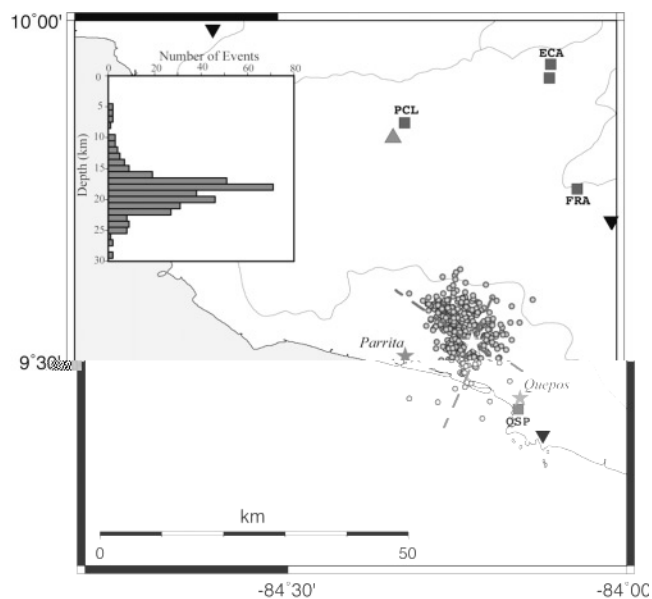


Figure 3. Relocated seismicity with HypoDD. Strong-motion stations are highlighted (square symbols). Thick, discontinuous lines give the trend of the two nodal planes from the Harvard CMT solution. Star marks the epicenter of the mainshock. Inset gives the depth distribution of relocated seismicity.

relocated events that were recorded during two previous seismic sequences in the same region as the Damas earthquake. The first seismic sequence was described by Güendel (1993) and occurred close to the town of Tarrazú, north of Quepos, in February 1989. The sequence started with a magnitude 4.4 and lasted for 3 weeks. The other sequence, located north of Parrita, started in December 1994, also with a 4.4 magnitude earthquake, and lasted through January 1995 (Fig. 4). After relocation, the 1989 sequence does not show an alignment of epicenters, but the final distribution is very similar to that described by Güendel (1993), who deployed portable instruments to better define the aftershock distribution. The 1994 sequence does show an alignment of epicenters along the Parrita fault, mapped by Marshall *et al.* (2000). These two earlier sequences are shallow, with earthquake depths distributed between the surface and 15 km.

Hence, the lack of alignment of epicenters for the Damas aftershock sequence most probably cannot be attributed to station distribution or location problems. Even the first 24 hr of aftershock hypocenters portray a pattern similar to that given by the 2 weeks of events (Fig. 3). Locations by the Red Sísmica Nacional of the University of Costa Rica–Instituto Costarricense de Electricidad (RSN) also show a similar aftershock distribution (Barquero and Rojas, unpublished report, 2004).

Regional CMT Inversion

The Tomography under Costa Rica and Nicaragua (TUCAN) experiment (Gonzalez *et al.* 2004), one project of the Subduction Factory initiative of MARGINGS (P. I. G. Abers and K. Fisher) deployed several portable broadband stations across northern Costa Rica and along the volcanic

axis during 2004 and 2005 (Fig. 2). We use the broadband records from the main event and the largest aftershocks to obtain their source mechanism by using a regional moment-tensor inversion (Randall *et al.*, 1995). In Table 1 we list the earthquakes and the regional CMT solutions obtained in this work, and in Figure 5 we show location and double-couple mechanism representations.

For the moment tensor inversion we bandpass filtered the observed displacement seismograms between 20 and 50 sec, except for the mainshock, which was bandpass filtered between 30 and 80 sec, and find the best moment tensor that minimizes the difference between the observed and synthetic seismograms in a least-squares sense. The minimum root-mean-square (rms) residual is searched through different centroid depths spaced every 5 km. Synthetic seismograms were generated with a reflectivity algorithm (Kennett, 1983; Randall, 1994) in the 1D crustal structure of Quintero and Kissling (2001).

Figure 6 shows an example of the observed and predicted synthetic seismograms for a late aftershock of June 2005. In general, we find a good match of the observed and synthetic seismograms and a reasonable agreement between polarities of *P*-wave first motion and the double-couple solution of the regional moment tensor inversion. Because most of the TUCAN stations lie to the northwest, first-motion *P*-wave polarities are crossed by one nodal plane.

For the mainshock, the regional solution agrees with the mechanism determined by Harvard, but we obtained a lower moment magnitude (M_w 6.2). Surface waves recorded at local and regional distances lack of the long-period energy recorded at teleseismic distances, giving lower moment magnitudes for moderate to large earthquakes. The nodal planes found with the regional inversion fit the *P*-wave first-

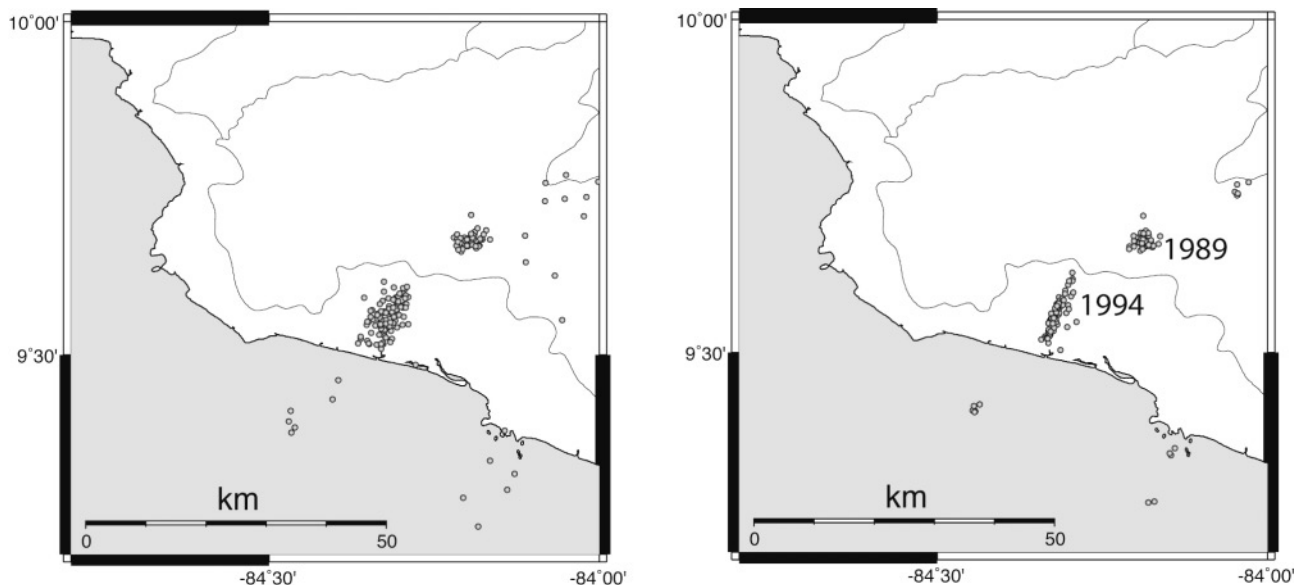


Figure 4. Selected (left) and relocated (right) seismicity for earthquake sequences of 1989 and 1994.

Table 1
Mainshock and Aftershock Regional CMT Solutions
from This Work

No.	Date		Latitude	Longitude	Depth	M_w	Strike	Dip	Rake
	(yy/mm/dd)	Time							
1	04/11/20	08:07	9.526	-84.210	23.3	6.2	208	44	-18
2	04/11/20	10:57	9.486	-84.260	17.3	4.3	53	74	-16
3	04/11/20	14:08	9.556	-84.250	20.0	4.5	201	33	-67
4	04/11/21	08:44	9.458	-84.252	21.3	4.5	169	49	-103
5	04/11/22	04:48	9.538	-84.254	28.4	4.2	90	53	133
6	04/12/07	08:15	9.459	-84.173	21.5	4.4	10	77	-14
7	05/06/23	15:15	9.531	-84.210	20.0	4.4	319	85	151

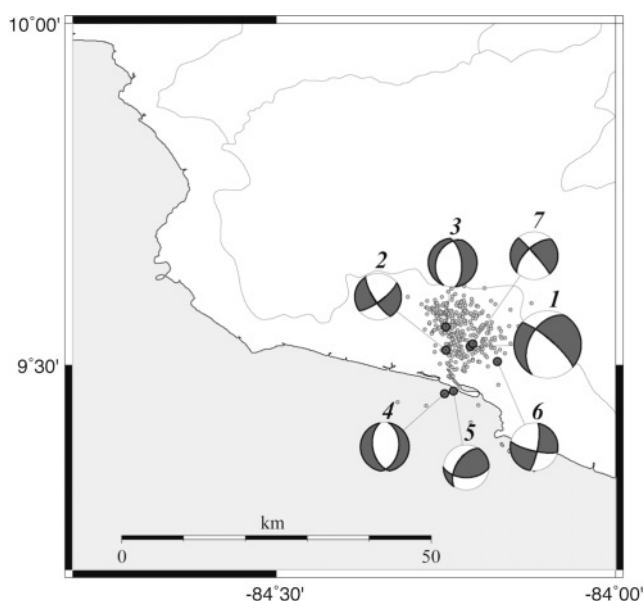


Figure 5. Regional CMT solutions. Location and double-couple mechanism of the main shock and largest aftershocks obtained from the Regional CMT. Numbers follow numeration in Table 1.

motion polarities better than Harvard's solution. The best centroid depth lies between 20 and 25 km.

None of the large aftershocks that occur immediately after the mainshock have mechanisms similar to that of the mainshock. Only a late aftershock that occurred in June 2005 (event 7 in Table 1) that locates very close to the mainshock hypocenter has a mechanism similar to that of the main event. Two aftershocks (3 and 4) occurred on a pure normal fault striking north and two aftershocks (2 and 6) show strike-slip mechanisms on left-lateral faults striking north-northeast or right-lateral striking west-northwest. Event 5 (Table 1) locates deeper (28 km) and might be associated with the plate interface. The solution for this event differs from the rest of the solutions because of its steep T axis. The event occurs on a steeply dipping reverse fault.

Simultaneous Inversion of Teleseismic and Local Records for Slip Distribution

Teleseismic P waves, retrieved from the Incorporated Research Institutions for Seismology Data Management Center web site, are used in conjunction with three strong-motion records to invert for the slip distribution on each one of the nodal planes. We followed the procedure described by Yagi *et al.* (2004) to obtain the best distribution of slip on each one of the nodal planes. A total of 18 teleseismic records were selected from stations located between 30° and 90° from the epicenter, and for uniform azimuthal coverage. We use 40 sec of recordings that contain P -wave and depth phases (pP and sP). Seismograms were bandpass filtered between 1 Hz and 80 sec and then converted into ground displacement. For the near-field data we selected the three closest stations (QSP, FRA, and ECA; Fig. 3) with good records after integration to ground displacement. Records were bandpass filtered from 20 sec to 0.5 Hz and integrated to ground displacement after being windowed to 40 sec long.

The fault plane was subdivided into 11 subfaults of $2 \text{ km} \times 2 \text{ km}$ in area. The initial rupture was constrained to the hypocenter and the rise time to 0.25 sec after performing a search for the minimum residual between observed and predicted seismograms using different rise-time values. Slip vector was constrained to that given by the Harvard best double-couple solution.

The results of the inversion are presented in Figure 7. The slip distribution is similar for both fault planes and resembles a simple circular rupture. Source time functions (STFs) do differ a little; the STF of the 204° plane is more spiky than the STF of the 305° nodal plane. Waveform matching is very similar, given similar variance and Akaike-Bayesian information criteria (ABIC), the two criteria to define a good fit of the synthetic seismograms to the observed waveforms (Yagi *et al.*, 2004), with a slightly better fit for the 204° striking nodal plane. Given the size of the earthquake (both solutions give M_w 6.5, a little larger than the value given by Harvard) and the lack of a strong directivity, it is not possible, with these data alone, to distinguish between the two nodal planes.

In general, a good agreement exists between the observed seismograms and the synthetic ones generated by the slip models (Fig. 8). Crustal structure variations, including lateral heterogeneities, and local site effects that are not taken into account, might be responsible for the better reproduction of the teleseismic records than those recorded in the near field.

Results of the inversion exhibit a rupture that lasted for about 6 sec and broke a circular asperity with a radius of 8 km. Average slip on the fault was 0.25 m and the largest slip of 0.8 m occurred between 19 and 21 km depth (Fig. 7). For a seismic moment of $7.6 \times 10^{18} \text{ N m}$ (M_w 6.5) and a rigidity of $7.23 \times 10^{10} \text{ N m}^{-2}$, we obtain an average stress drop on the fault of 60 bars.

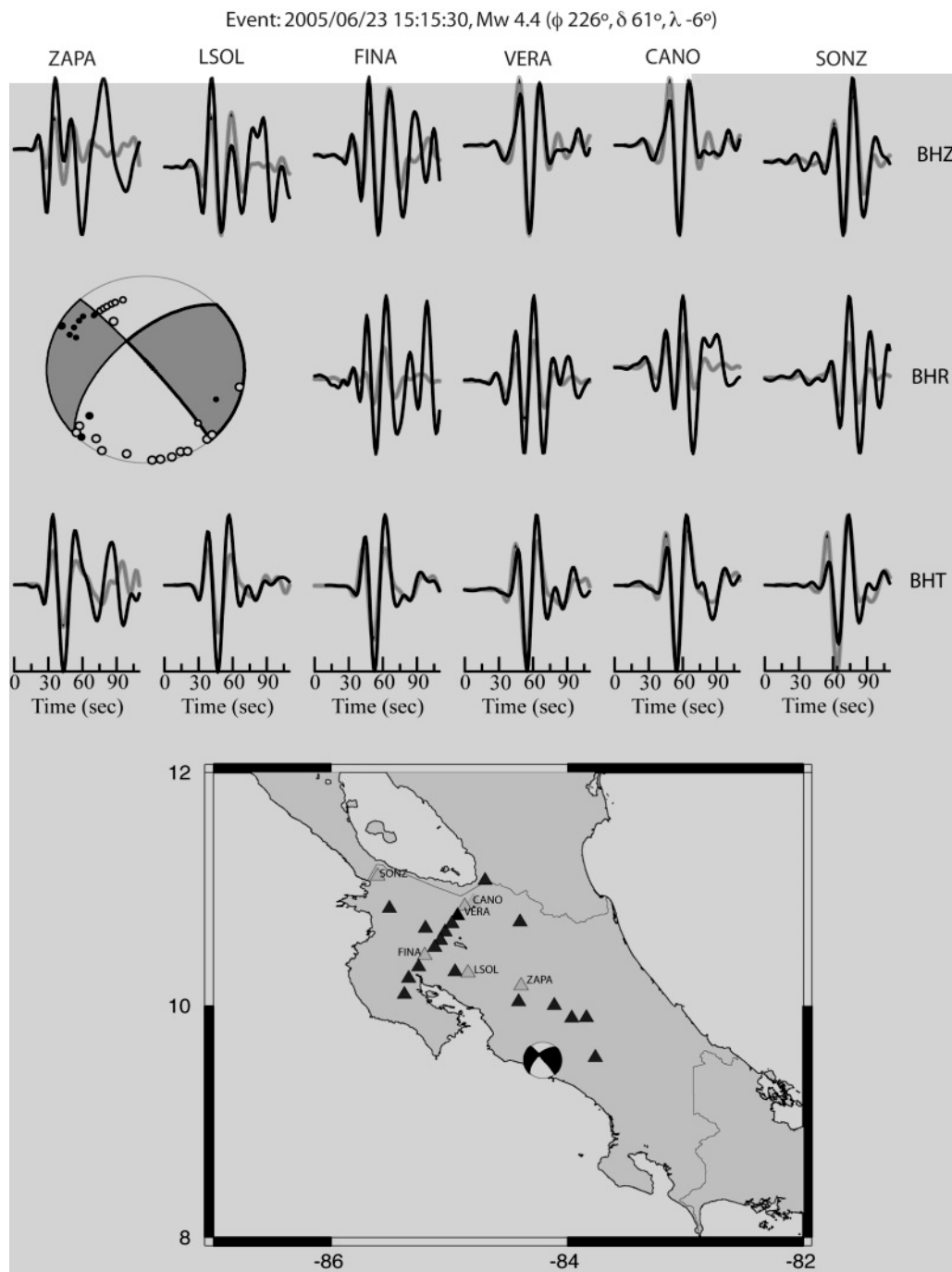


Figure 6. (Top) Observed seismograms (thick black line) and synthetic seismograms (thick gray line) for the mechanism on the left. First-motion P -wave polarities are shown as compressions (dark points) and dilatations (open circles) on the focal sphere. Lower map shows the location of the stations from the TUCAN array used in the inversion.

Empirical Green's Functions

None of the large aftershocks following the Damas earthquake have a mechanism similar to the main event, but a late aftershock (Table 1) that occurred in June 2005 has both a mechanism and location similar to the main event.

This late earthquake of magnitude 4.4 can be used as an empirical Green's function to retrieve the apparent source time function (ASTF) from recordings at stations of the TUCAN array. Because of saturation of surface waves in most of the recordings from the main event, we use the PnI train of phases, from the vertical seismograms, to obtain the

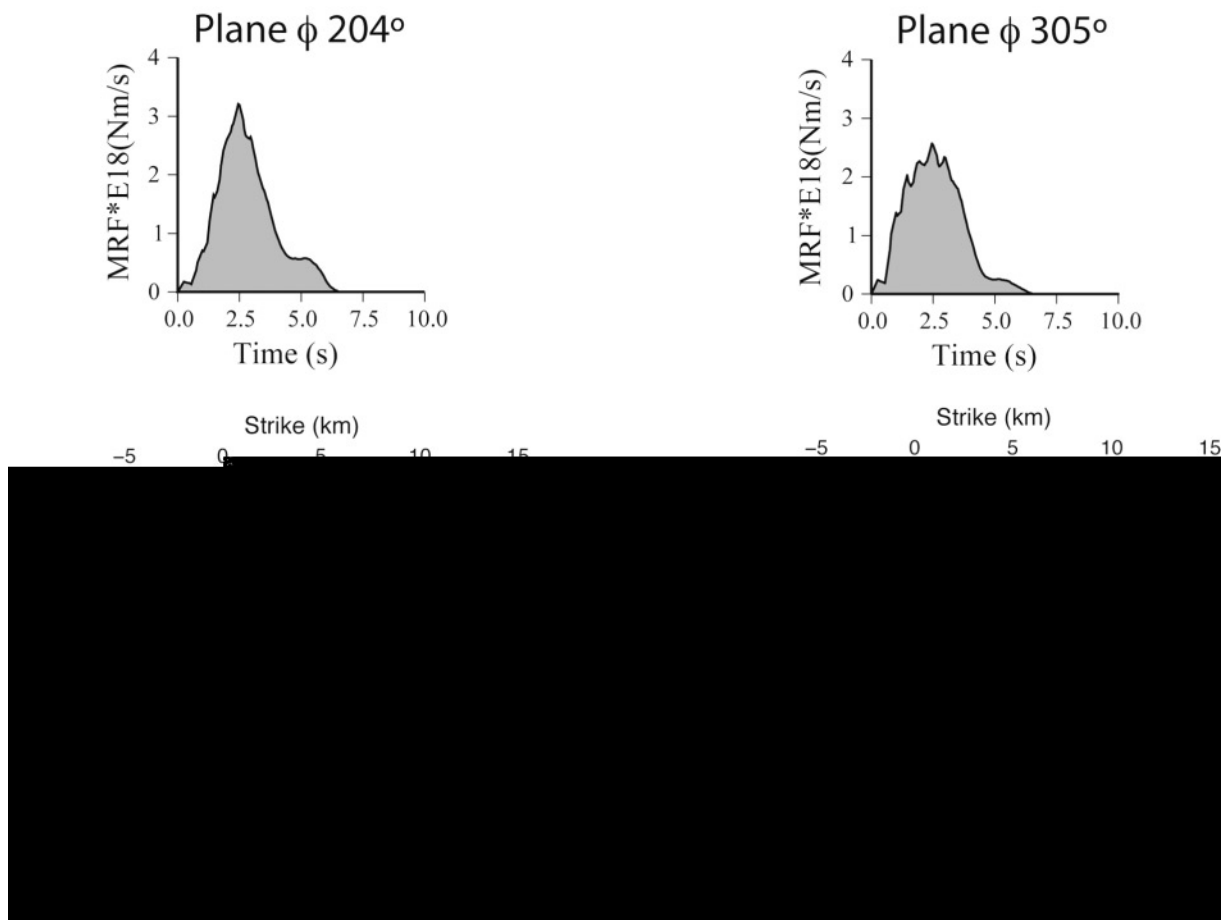


Figure 7. Teleseismic and local inversion for the slip distribution. STF (top) obtained from the inversion and slip distribution (bottom) on the fault plane (204° on the left and 305° on the right). Arrows show the slip vector direction.

ASTFs at several stations. Figure 9 shows the ASTFs calculated from deconvolving 10 sec of the P -wave group of the aftershock to the mainshock. We used a time-domain deconvolution (Ligorria and Ammon, 1999) and applied a gaussian filter with a half-width of 1 sec. Unfortunately, the aftershock is not an exact replica of the mainshock; nodal planes differ by about 10° (Fig. 9). Although stations very close to the nodal plane have different P -wave first-motion polarities, waveforms of a station far from the nodal planes are very similar, and deconvolution is very stable for these seismograms.

We have two quadrants of the focal sphere covered by the TUCAN array, but just a few stations are away from the nodal planes. ASTFs at stations HDC5, COVE, TABL, and CANO are very similar, they plot away from the nodal planes and they plot close to each other on the focal sphere, whereas CABA and MANS differ from them and locate very close to the nodal plane of the main event (gray color on Fig. 9).

In Figure 10 we compare the ASTFs computed at the two nodal planes using the slip distribution obtained from

the teleseismic and local recording inversion, with the ASTFs obtained from the deconvolution. Both functions were normalized for comparison. The left side of Figure 10 shows the observed ASTF in thin line and the computed ASTF from the slip distribution for the nodal plane striking 204° with a thick line. At the right side, we show the results for the nodal plane striking 305° . For the stations that locate far from the nodal planes, the ASTFs computed with the slip distribution for plane striking 305° fit better the observed ASTF. The ASTF computed with the slip distribution for plane striking 204° are wider than the observed functions. ASTFs for the other two stations differ considerably from those calculated from the slip distributions, with the ASTF calculated for the plane striking 204° fitting better the observed ASTFs.

Again, it is not possible to determine the rupture plane with the regional data alone, although there is a preference for the plane striking 305° just by the similarity between ASTFs generated from the slip distribution and the observed ASTFs from stations that plot away from the nodal planes in the focal sphere.

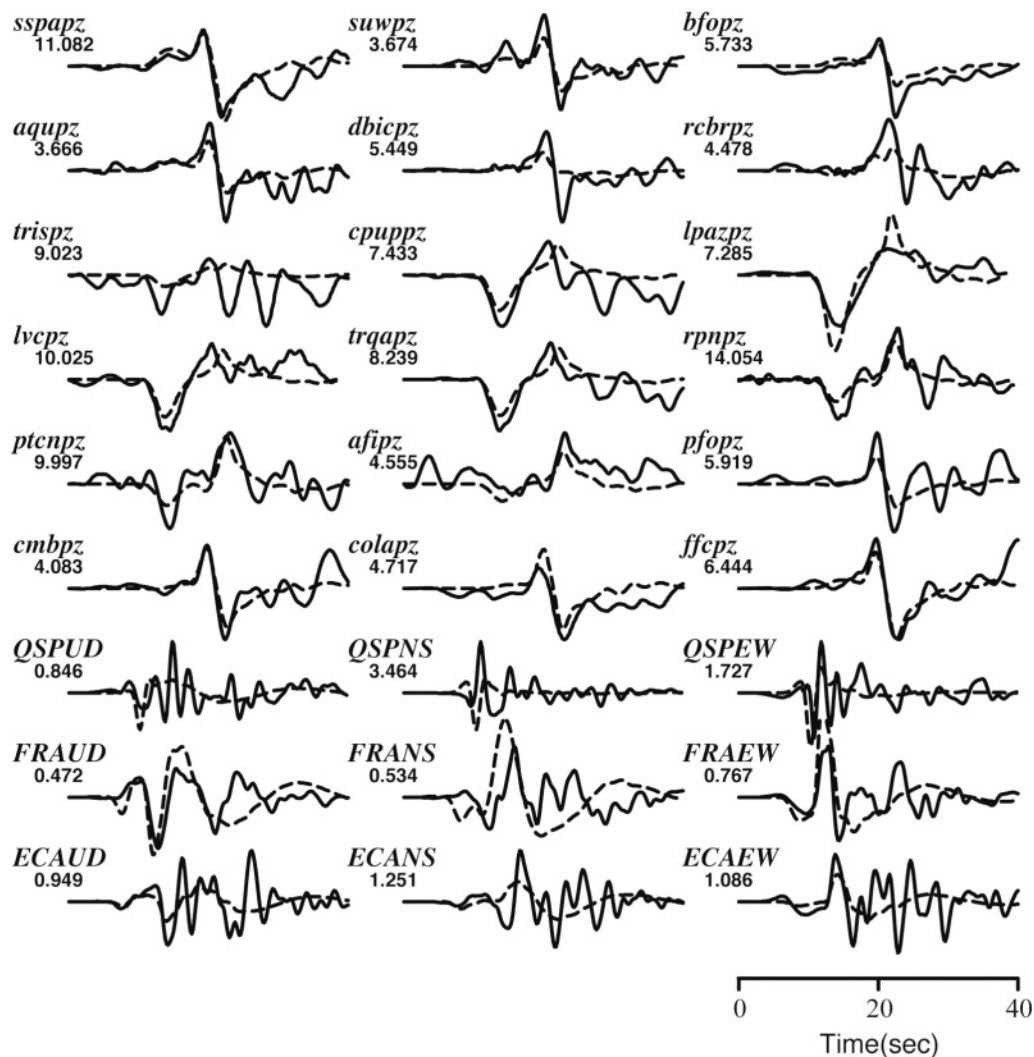


Figure 8. Observed (continuous line) and synthetic (dashed line) seismograms modeled after the slip distribution obtained for the plane striking 204° . Numbers below the station name are maximum amplitude.

Discussion

Aftershock hypocenters of the Damas earthquake are distributed between 15 and 25 km, with a peak in their distribution at about 18 km. The hypocenter of the main event was located at 24 km and the rupture extended from 12 to 25 km in depth, having the maximum slip at about 20 km. Hence, the Damas earthquake occurred between mid and low crustal depths and probably just above the plate interface between the Cocos plate and the Panama microplate. Slip does not reach the surface. The slip distribution resembled that of a simple circular rupture, with a radius of 8 km, and produced an average stress drop of 60 bars.

Given the size of this earthquake, at the limit of resolution for teleseismic data, the poor distribution of near-field and regional stations, it was not possible to distinguish the fault plane from the auxiliary plane. Nevertheless, knowing the predilection of surface faults on the forearc to strike to

the northeast (Marshall *et al.*, 2000), the causative fault was most probably a left-lateral fault, striking 204° from the north. This type of margin-perpendicular fault is responsible for the uplift of fault-bounded blocks, probably related to the subduction of rough seafloor and underplating of seamounts (Fisher *et al.*, 1994, 1998; Marshall *et al.*, 2000).

The other plane, striking 305° , cannot be ruled out as the causative fault, as similar oriented faults dominate the volcanic arc, the region to the north, and some of them have been mapped in the forearc.

The depth of the hypocenter of the main event, the aftershock, and slip distribution, and the shallow location of the plate interface in central Pacific Costa Rica, suggests that the source of the rupture has deep roots into the subducted lithosphere. Basal traction on the overriding plate from young and buoyant oceanic plate with rough seafloor causes horizontal shortening and shear on the upper plate (e.g., Fisher *et al.*, 1998; Marshall *et al.*, 2000).

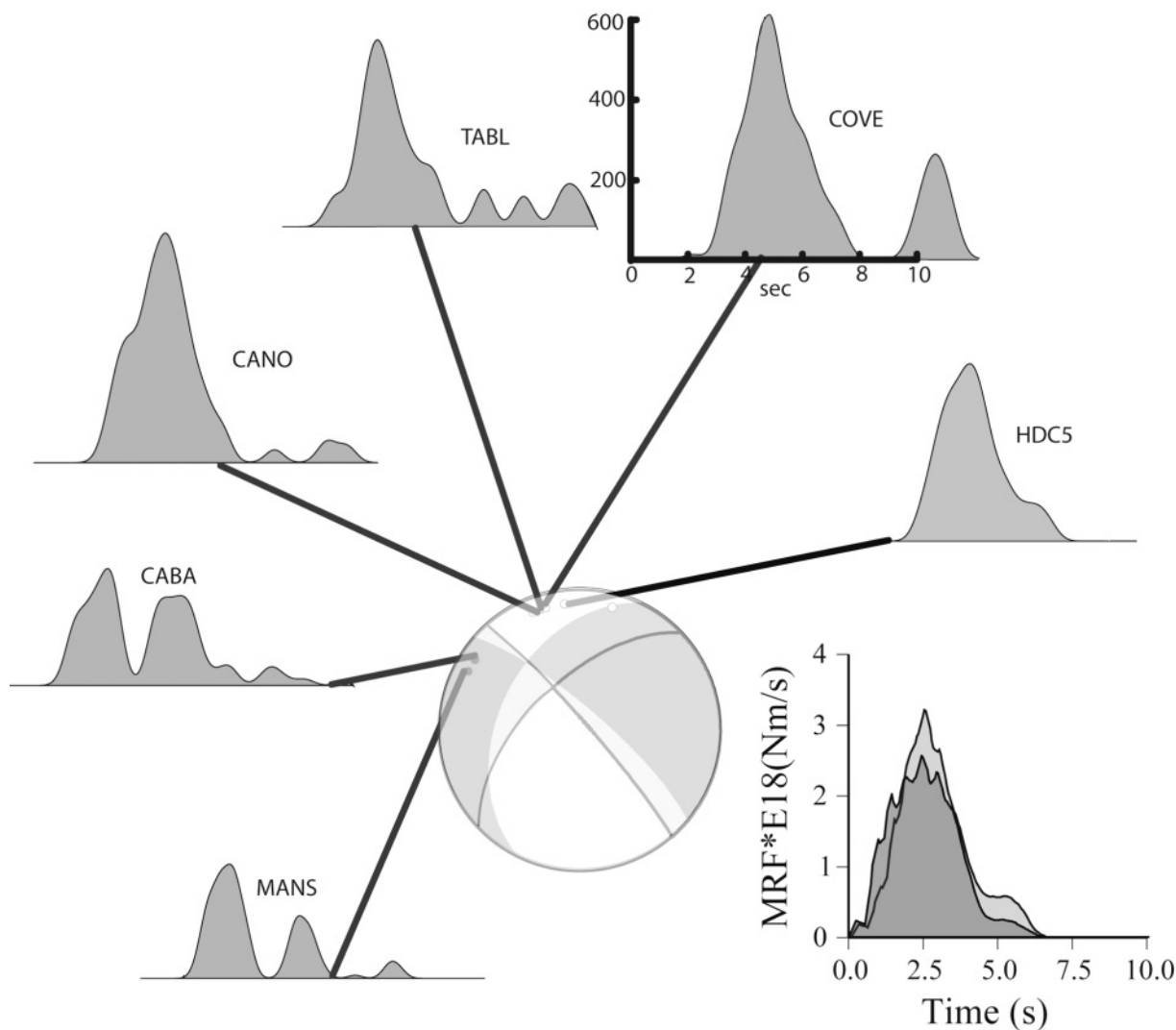


Figure 9. Apparent STFs. Fault plane solution for the mainshock (gray color) and aftershock (thick lines). ASTF obtained from deconvolution of the P -wave and P -wave coda. STFs obtained from the teleseismic inversion are shown on the lower right for comparison.

The hypocenter of this earthquake is located deep into the lower crust where temperature and lithostatic stresses might be too high for brittle failure. If high pore pressures dominate the lower crust, we would expect this high pore pressure to diminish the effective normal stress on the fault and produce brittle failure at this depth. Combined on- and offshore wide-angle seismic data (Stavenghagen *et al.*, 1998) show a thick (5 km), low-velocity layer above the slab. The low velocity of the layer might be explained from highly fractured material eroded from the margin wedge (Vannucchi *et al.*, 2003), underplated material from the top of seamounts, sediments, and fluids. Fluids released from this layer by increasing depth and temperatures migrate upward, increasing pore pressure at depths between 15 and 25 km. Although thick, low-velocity zones are not well constrained with just wide-angle seismic data, tomographic studies by

Husen *et al.* (2003) find a large low-velocity segment within and above the slab in Central Costa Rica, below the coast (see their sections CC' and DD'), which could be interpreted as hydrous rocks. Also DeShon *et al.* (2003) found a thin, low-velocity oceanic crust in their tomographic models of the Central Costa Rica subduction zone. Fluids migrate upward through fractures in the lower crust generated by seamount subduction.

Five early aftershocks were studied here and they show mechanisms very different from the mainshock. Nevertheless, T axes from six events listed in Table 1 have the characteristic direction in the forearc, described by Marshall *et al.* (2000), with shallow T axes trending almost east-west. Event 5, which might be associated with the plate interface, has an almost vertical T axis. With all the diverse mechanisms found for the largest aftershocks, it is not surprising

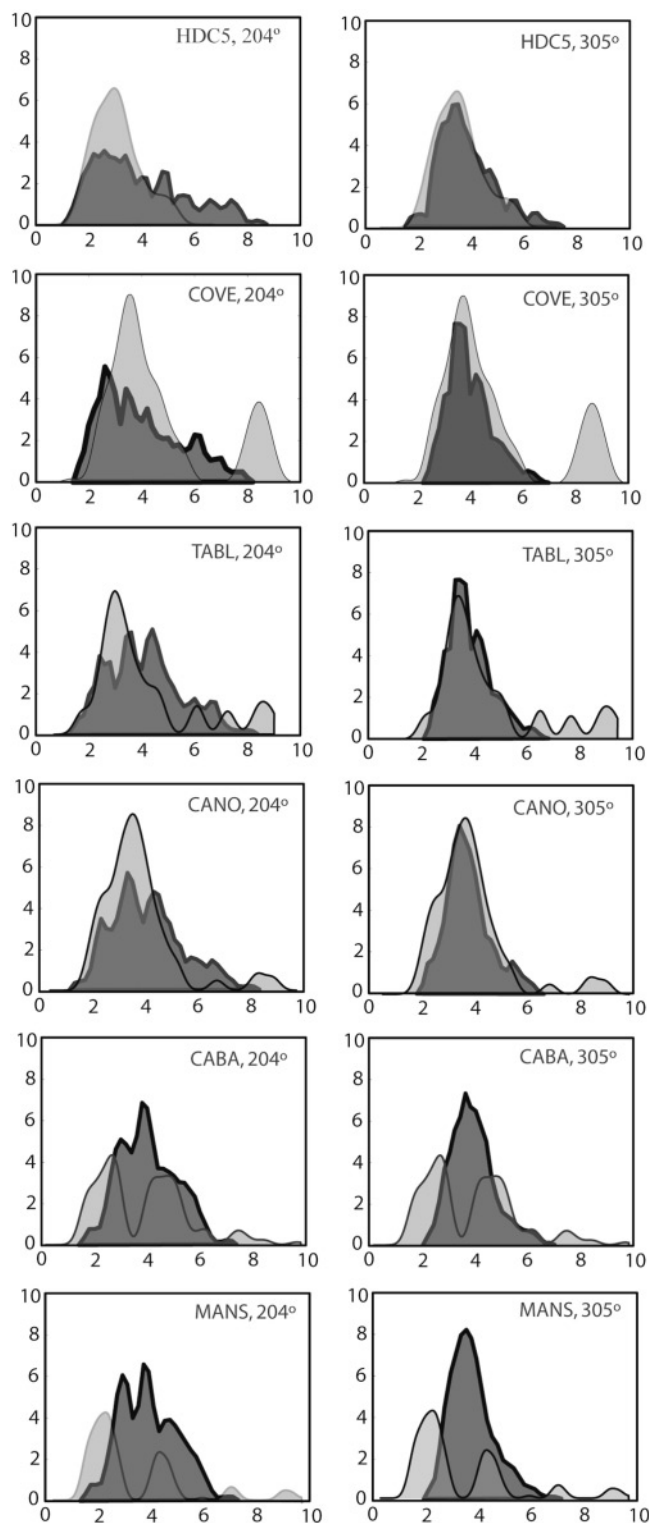


Figure 10. Comparison between ASTF computed at the two nodal planes using the slip distribution obtained from the teleseismic and local recording inversion, with those obtained from the deconvolution. ASTF obtained from deconvolution in light gray and the one obtained from the results of the teleseismic inversion in darker color and thicker lines. On the left are the results for the 204° nodal plane, and the right for the 305° nodal plane.

to find an absence of pattern in the aftershock distribution. Rupture on the main fault triggered slip on adjacent faults, some of them having the same trend and slip direction as the mainshock, but others have dip-slip or sinistral motion on north-south-oriented faults. Aftershocks projected onto the nodal planes are distributed close to where most of the seismic moment was released during the mainshock (Fig. 11). For the nodal plane striking 204° from north, the aftershocks are distributed perpendicular to the fault plane (Fig. 11, lower left), whereas for the 305° nodal plane, the aftershocks are distributed as a volumetric source around the area with the largest slip during the mainshock (Fig. 11, right). High pore pressure might also explain the volumetric distribution of aftershocks for this earthquake. Whereas shallow seismicity, like the 1994 sequence on the Parrita fault, locates along a line or superficial fault, aftershocks of the Damas event do not lie on a plane. Rupture after the mainshock releases pore pressure on the fault plane, inhibiting brittle failure on the same fault, but increasing shear stress on adjacent segment rocks with high pore pressure, which can produce brittle fracture.

Conclusions

The M_w 6.4 event of 20 November 2004 was located north of Damas Island in the Pacific coastal area of Costa Rica. Hypocenter location, slip, and aftershock-depth distribution place this event inside the lower crust, just above the plate interface between two converging tectonic plates. The earthquake locates within the CCRDB, in a forearc highly deformed by subduction of an over thickened and buoyant oceanic plate with rough seafloor. The mechanism of the main event has strike-slip motion on a sinistral fault trending southwest or dextral motion on a fault trending northwest. Because of its small size and circular rupture, no preference for either of the nodal planes can be found from aftershock distribution, teleseismic, regional, or local data. The main event rupture lasted for 6 sec, had a maximum slip of 0.8 m, an average of 0.25 m on a circular fault of 8 km radius, for an average stress drop of 60 bars.

As evidenced from this earthquake, its slip distribution, hypocenter location, and aftershock depth distribution, and from mapped faults at the surface, deformation due to rough seafloor and seamounts, takes place across the entire crust in the Central Costa Rica forearc.

Acknowledgments

We are grateful to Daniel Rojas and Antonio Mata for maintaining the OVSICORI seismic network. The data collected by the TUCAN array were of great help and we thank all the participants in this experiment. Strong-motion records were obtained from the Laboratorio de Ingeniería Sísmica from the Instituto de Investigaciones en Ingeniería of the University of Costa Rica, we thank all the staff of the Laboratorio for providing good quality, near-field, strong ground motion recordings. All the figures were produced with the software provided by the GMT software package described by Wessel and Smith (1998). We thank Marino Protti and Karen

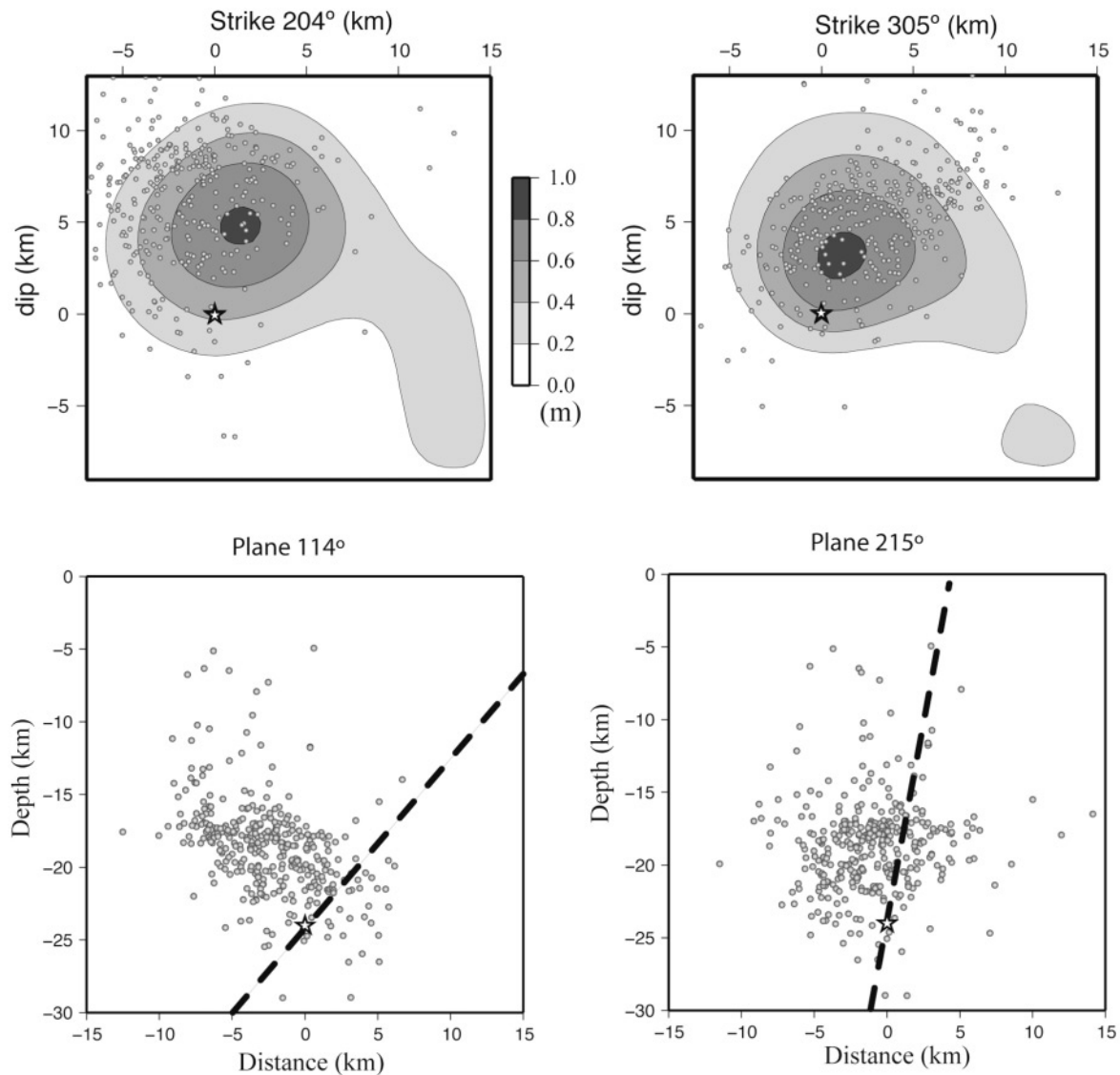


Figure 11. Aftershock hypocenters and slip distribution on each one of the nodal planes and on a cross section perpendicular to each nodal plane.

McNally for insightful discussions that helped us improve this manuscript. We also thank S. Husen for a useful discussion on his tomographic studies in the area.

References

- Arias, O., and P. Denyer (1991). Estructura geológica de la región comprendida en las hojas topográficas Abras, Caraiques, Candelaria y Río Grande, Costa Rica, *Rev. Geol. Am. Cent.* **12**, 61–74.
- Barkhausen, U., C. R. Ranero, R. von Huene, S. C. Cande, and H. A. Roeser (2001). Revised tectonic boundaries in the Cocos Plate off Costa Rica: implications for the segmentation of the convergent margin and for plate tectonic models, *J. Geophys. Res.* **106**, 19,207–19,220.
- DeMets, C., R. G. Gordon, D. F. Argus, and S. Stein (1990). Current plate motions, *Geophys. J. Int.* **101**, 425–478.
- Denyer, P., W. Montero, and G. E. Alvarado (2003). Atlas Tectónico de Costa Rica, Editorial Universidad de Costa Rica, serie Reportes Técnicos, Costa Rica, 81 pp.
- DeShon, H. R., S. Y. Schwartz, S. L. Bilek, L. M. Dorman, V. Gonzalez, J. M. Protti, E. R. Flueh, and T. H. Dixon (2003). Seismogenic zone structure of the southern Middle America Trench, Costa Rica, *J. Geophys. Res.* **108**, B10, 2491, doi 10.1029/2002JB002294.
- Fernández, M. (1996). Evaluación del hipotético sistema de falla transcurriente este-oeste de Costa Rica, *Rev. Geol. Am. Cent.* **19/20**, 57–74.
- Fernández, M., and J. Pacheco (1998). Sismotectónica de la región central de Costa Rica, *Rev. Geol. Am. Cent.* **21**, 5–23.
- Fisher, D. M., T. W. Gardner, J. S. Marshall, and W. Montero (1994). Kinematics associated with late Cenozoic deformation in central Costa Rica: western boundary of the Panama microplate, *Geology* **22**, 263–266.
- Fisher, D. M., T. W. Gardner, J. S. Marshall, P. B. Sak, and M. Protti (1998). Effect of subducting seafloor roughness on fore-arc kinematics, Pacific coast, Costa Rica, *Geology* **26**, 467–470.
- Gonzalez, V., M. Protti, K. M. Fisher, C. A. Rychert, A. Walker, G. A. Abers, L. Auger, E. Syracuse, and T. A. Plank (2004). Preliminary earthquake locations from the Costa Rica component of the TUCAN network, *EOS Trans AGU* **85**, no. 47 (Fall Meet. Suppl.).

- Güendel, F. (1993). Secuencia sísmica de el alto del Aguacate Febrero y Marzo de 1989, Cat. De Temblores OVSICORI-UNA, 155–161.
- Güendel, F., K. C. McNally, J. Lower, M. Protti, R. Saenz, E. Malavassi, J. Barquero, R. Van der Laat, V. Gonzalez, C. Montero, E. Fernández, D. Rojas, J. de Dios Segura, A. Mata, and Y. Solis (1989). First results from a new seismographic network in Costa Rica, Central America, *Bull. Seism. Soc. Am.* **79**, 205–210.
- Harvard Seismology (2005). Centroid Moment Tensor (CMT) catalog search, www.seismology.harvard.edu/ (last accessed ●●●).
- Hey, R. (1977). Tectonic evolution of the Cocos-Nazca spreading center, *Geol. Soc. Am. Bull.* **88**, 1404–1420.
- Husen, S., E. Kissling, and R. Quintero (2002). Tomographic evidence for a subducted seamount beneath the Gulf of Nicoya, Costa Rica: the cause of the 1990 $M_w = 7.0$ Gulf of Nicoya earthquake, *Geophys. Res. Lett.* **29**, doi 10.1029/2001GL014045.
- Husen, S., R. Quintero, E. Kissling, and B. Hacker (2003). Subduction-zone structure and magmatic processes beneath Costa Rica constrained by local earthquake tomography and petrological modelling, *Geophys. J. Int.* **155**, 11–32.
- Kennett, B. L. N. (1983). *Seismic Wave Propagation in Stratified Media*, Cambridge University Press, Cambridge, U.K., 342 pp.
- Lienert, B. R., and J. Haskov (1995). A computer program for locating earthquakes both locally and globally, *Seism. Res. Lett.* **66**, 26–36.
- Ligorria, J. P., and C. J. Ammon (1999). Iterative deconvolution and receiver-function estimation, *Bull. Seism. Soc. Am.* **89**, 1395–1400.
- Marshall, J. S., D. M. Fisher, and T. W. Gardner (2000). Central Costa Rica deformed belt: kinematics and diffuse faulting across the western Panama block, *Tectonics* **19**, 468–492.
- Montero, W. (1999). El terremoto del 4 de Marzo de 1924 (M_s 7.0): ¿Un gran temblor interplaca relacionado al límite incipiente entre la Placa Caribe y la Microplaca de Panamá? *Rev. Geol. Am. Cent.* **22**, 25–62.
- Protti, M., F. Güendel, and K. McNally (1994). The geometry of the Wadati-Benioff zone under southern Central America and its tectonic significance: results from a high-resolution local seismographic network, *Phys. Earth Planet. Interiors* **84**, 271–287.
- Protti, M., F. Güendel, and K. McNally (1995a). Correlation between the age of the subducting Cocos plate and the geometry of the Wadati-Benioff zone under Nicaragua and Costa Rica, in *Geologic and Tectonic Development of the Caribbean Plate Boundary in Southern Central America*, P. Mann (Editor), Geol. Soc. Am. Special Pap. 295, 309–326.
- Protti, M., K. McNally, J. Pacheco, V. Gonzales, C. Montero, J. Segura, J. Brenes, V. Barboza, E. Malavassi, F. Güendel, G. Simila, D. Rojas, A. Velasco, A. Mata, and W. Schillinger (1995b). The March 25, 1990 ($M_w = 7.0$, $M_L = 6.8$) earthquake at the entrance of the Nicoya Gulf, Costa Rica: its prior activity, foreshock, aftershocks, and triggered seismicity, *J. Geophys. Res.* **100**, no. B10, 20,345–20,358.
- Quintero, R., and E. Kissling (2001). An improved P-wave velocity reference model for Costa Rica, *Geofis. Int.* **40**, 3–19.
- Randall, G. E. (1994). Efficient calculation of complete differential seismograms for laterally homogeneous earth models, *Geophys. J. Int.* **118**, 245–254.
- Randall, G. E., C. J. Ammon, and T. J. Owens (1995). Moment tensor estimation using regional seismograms from a Tibetan plateau portable network deployment, *Geophys. Res. Lett.* **22**, 1665–1668.
- Stavenhagen, A. U., E. R. Flueh, C. Ranero, K. D. McIntosh, T. Shipley, G. Leandro, A. Schulze, and J. J. Dañoibeitia (1998). Seismic wide-angle investigations in Costa Rica—a crustal velocity model from the Pacific to the Caribbean coast, *Zbl. Geol. Palaont. Teil I* **1997**, 393–408.
- Vannucchi, P., C. R. Ranero, S. Galeotti, S. M. Straub, D. W. Scholl, and K. McDougall-Ried (2003). Fast rates of subduction erosion along the Costa Rica Pacific margin: Implications for nonsteady rates of crustal recycling at subduction zones, *J. Geophys. Res.* **108**, no. B11, 2511, doi 10.1029/2002JB002207.
- von Huene, R., J. Hoffmann, P. Holler, R. Leon, O. Barrios, J. Chavarría, J. Jeschke, and D. Escobedo (1995). Morphotectonics of the Pacific Convergent Margin of Costa Rica, in *Geological and Tectonic Development of the Caribbean Plate Boundary in Southern Central America*, Geol. Soc. Am. Special Pap. 295, 291–307.
- von Huene, R., C. R. Ranero, W. Weinrebe, and K. Hinz (2000). Quaternary convergent margin tectonics of Costa Rica, segmentation of the Cocos Plate, and Central American volcanism, *Tectonics* **19**, 314–334.
- Waldhauser, F., and W. L. Ellsworth (2000). A double-difference location algorithm: method and application to the Northern Hayward Fault, California, *Bull. Seism. Soc. Am.* **90**, 1353–1368.
- Werner, R., K. Hoernle, P. van den Bogaard, C. R. Ranero, R. von Huene, and D. Korich (1999). A drowned 14 m.y.-old Galapagos archipelago off the coast of Costa Rica: implications for tectonic and evolutionary models, *Geology* **27**, 499–502.
- Wessel, P., and W. Smith (1998). New, improved version of Generic Mapping Tools released, *EOS* **179**, 579.
- Yagi, Y., T. Mikumo, J. Pacheco, and G. Reyes (2004). Source rupture process of the Tecoman, Mexico earthquake of 22 January 2003, determined by joint inversion of Teleseismic body-wave and near-source data, *Bull. Seism. Soc. Am.* **94**, 1795–1807.

Instituto de Geofísica
 Universidad Nacional Autónoma de México
 Ciudad Universitaria, Delegación Coyoacán
 CP 04510, Ciudad de México, México
 javier@ollin.igeofcu.unam.mx
 (J.F.P.)

Observatorio Vulcanológico y Sismológico de Costa Rica
 Universidad Nacional
 Heredia, Costa Rica
 (J.F.P., R.O., F.V., J.S., W.J., V.G.)

Manuscript received 20 December 2005.